Absence of ferromagnetism in MnBi₂Te₄/Bi₂Te₃ down to 6 K

T. Fukasawa, ¹ S. Kusaka, ¹ K. Sumida, ^{1,2} M. Hashizume, ¹ S. Ichinokura, ¹ Y. Takeda, ² S. Ideta, ³ K. Tanaka, ³ R. Shimizu, ⁴ T. Hitosugi, 4 and T. Hirahara 1,*

> ¹Department of Physics, Tokyo Institute of Technology, Tokyo 152-8551, Japan ²Materials Sciences Research Center, Japan Atomic Energy Agency, Sayo, Hyogo 679-5148, Japan ³UVSOR Facility, Institute for Molecular Science, Okazaki 444-8585, Japan ⁴School of Materials and Chemical Technology, Tokyo Institute of Technology, Tokyo 152-8550, Japan



(Received 16 November 2020; accepted 20 April 2021; published 4 May 2021)

We successfully fabricated a MnBi₂Te₄/Bi₂Te₃ heterostructure by incorporating Mn and Te inside the topmost quintuple layer of Bi₂Te₃, as unambiguously confirmed by low-energy electron diffraction I-V and scanning transmission electron microscopy measurements. The surface-state Dirac cone of the heterostructure showed little change compared to that of pristine Bi₂Te₃, and x-ray magnetic circular dichroism measurements showed that the system was paramagnetic down to 5.6 K. These results are in contrast to previous works on related materials that showed magnetic order around 10 K as well as theoretical predictions and suggest the intricacy of the magnetic properties of two-dimensional van der Waals magnets.

DOI: 10.1103/PhysRevB.103.205405

I. INTRODUCTION

Since their discovery in 2017, two-dimensional van der Waals (2D vdW) ferromagnets have attracted considerable attention since they are expected to possess peculiar magnetic properties compared to the parent bulk compound [1,2]. Nowadays, numerous materials have been fabricated by exfoliation or thin-film growth, and the relationship between magnetism and other long-range order such as charge density waves has been explored [3]. The tunability of the magnetic properties has also been discussed by applying external stimulus or changing the thickness [4]. However, there is still much debate about the intrinsic property of the thinnest 2D vdW materials with the least number of magnetic layers (ideally, a single magnetic layer) inside. For example, single-layer VSe₂ was initially reported to host ferromagnetism up to room temperature [5,6], but later, other works showed the absence of magnetic order down to low temperatures [7,8]. The discrepancy between different reports has not been systematically clarified up to now, but the deviation in the substrate or the growth conditions (stoichiometry or the film quality) may be one factor [9].

These 2D vdW ferromagnets are also promising in the context of inducing magnetism into topological insulators (TIs) by forming heterostructures. For example, the Cr₂Ge₂Te₆/(Bi,Sb)₂Te₃ system was shown to exhibit a large anomalous Hall effect due to the large magnetic proximity effect at the interface [10]. Furthermore, there are some 2D vdW materials in which the magnetic layers are inserted into the TI itself by self-organization such as MnBi₂Se₄ and MnBi₂Te₄ [11]. In these systems, a single Mn layer with magnetic moments is embedded inside Bi₂Se₃ or Bi₂Te₃ (magnetic extension of the TI) [12–14], and in the bulk form they are called intrinsic magnetic TIs [15,16]. There are also similar materials in which multiple n magnetic layers are embedded such as $Mn_nBi_2Se(Te)_{n+3}$, and their magnetic and structural properties have been discussed theoretically [17,18] as well as experimentally [19]. The relation between the inter or intra long-range order in the magnetic layers and the presence or absence of the surface Dirac-cone (DC) gap has been debated for such systems, and the connection between the two has been shown to be, indeed, quite complicated [15,19–26].

Therefore, in the present study, we aimed to investigate the magnetic properties of and their implication for the dispersion of the surface-state DC in one of the simplest systems among the magnetic topological heterostructures, namely, MnBi₂Te₄/Bi₂Te₃. After carefully identifying the atomic structure with low-energy electron diffraction (LEED) I-V analysis and scanning transmission emission microscopy (STEM) measurements, we performed x-ray magnetic circular dichroism (XMCD) and high-resolution angle-resolved photoemission (ARPES) measurements. We found that the heterostructure was paramagnetic down to 5.6 K and the DC dispersion showed little change compared to the pristine Bi₂Te₃ down to 16 K. These results contradict previous experimental works on bulk samples with multiple MnBi₂Te₄ layers, exfoliated MnBi₂Te₄ samples [27], and also theoretical calculations. They point to the importance of the supporting substrate or the presence of adjacent layers in discussing the magnetic properties of 2D vdW materials.

II. EXPERIMENT

The heterostructure samples were prepared by molecular beam epitaxy in ultrahigh vacuum (UHV) chambers equipped with a reflection high-energy electron diffraction (RHEED) system. First, a clean Si(111) 7×7 surface was prepared on

^{*}hirahara@phys.titech.ac.jp

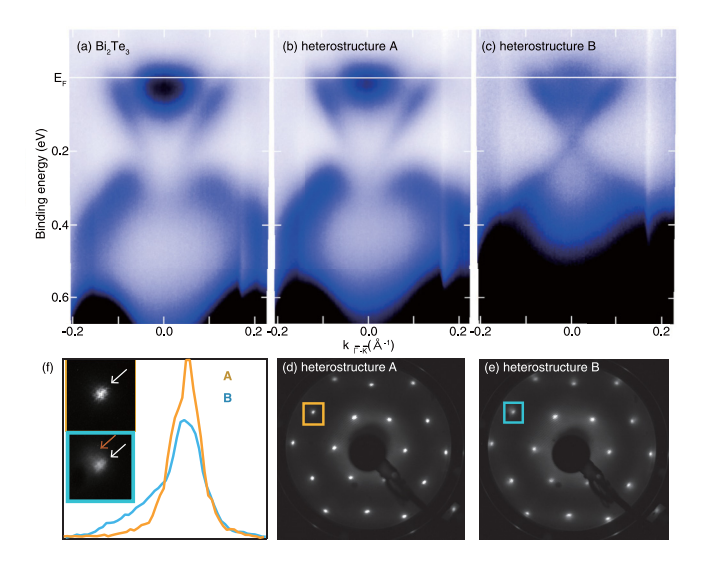


FIG. 1. The band structure of (a) the substrate Bi_2Te_3 film, (b) heterostructure A with 3 min of Mn and Te deposition on Bi_2Te_3 , and (c) heterostructure B with 8 min of Mn and Te deposition on Bi_2Te_3 . The dispersion shown is along the $\bar{\Gamma}$ - \bar{K} direction, and the measurements were performed at room temperature with $h\nu=21.2$ eV. LEED patterns of heterostructures (d) A and (e) B, taken at E=60 eV. (f) Line profiles of the (11) spot surrounded by the squares in (d) and (e). The insets show close-up images of the regions surrounded by squares, and the arrows indicate the spot positions.

an n-type substrate by a cycle of resistive heat treatments. Then Bi was deposited on the 7×7 substrate at $\sim 250\,^{\circ}\mathrm{C}$ in a Te-rich condition. Such a procedure is reported to result in a smooth epitaxial film formation with a stoichiometric ratio of Bi:Te = 2:3. The grown Bi₂Te₃ films were annealed at $\sim 250\,^{\circ}\mathrm{C}$ for 5 min. The thickness of the Bi₂Te₃ films in this work is ~ 8 quintuple layers (QL). Finally, Mn was deposited on Bi₂Te₃ in a Te-rich condition at $\sim 260\,^{\circ}\mathrm{C}$. The 1×1 periodicity is maintained during this sample fabrication procedure, as discussed later.

ARPES measurements were performed *in situ* after the sample preparation with a commercial hemispherical photoelectron spectrometer equipped with angle and energy multidetections. We used two different apparatuses: Gammadata Scienta SES-100 in the laboratory with unpolarized HeI α (21.2 eV) radiation and MBS A1 at BL-7U of UVSOR-III using p-polarized photons in an energy range of 7.5–21 eV [28]. The measurements were performed at room temperature in the laboratory and at 16 K in UVSOR.

LEED measurements were also performed *in situ* after the sample formation in another UHV chamber at 100 K with Omicron SPECTALEED. The in-plane lattice constant of the heterostructure was determined from positions of the LEED spots as well as the RHEED spots.

For the XMCD and STEM measurements, the fabricated samples were first characterized with ARPES at room temperature. After confirming that the desired band dispersion was obtained (Fig. 1), they were capped with $\sim \! 10$ nm of Te before taking them out of the UHV chamber.

The x-ray absorption spectroscopy (XAS) and XMCD measurements were performed at BL-23SU of SPring-8 [29] with circularly polarized x-ray radiation. The total-electron

yield mode was employed in both cases. The Te-capped samples were annealed at $\sim 250\,^{\circ}\text{C}$ to remove the capping layers prior to the measurements.

Electron transparent specimens for STEM observations were prepared by the standard lift-out technique using an FEI Helios G4-UX dual-beam system. Probe aberration-corrected STEM, an FEI TitanG2 80-200 microscope, was used. Chemical compositions were measured by energy-dispersive x-ray spectroscopy (EDS).

III. RESULTS AND DISCUSSION

Figure 1(a) shows the typical band dispersion near the Fermi level E_F of the Bi₂Te₃ film measured at room temperature with hv = 21.2 eV photons. The surface DC as well as the bulk conduction band is observed. After deposition of Mn and Te, the band structure hardly changes at first, as revealed in Fig. 1(b). Only a slight increase in the Fermi wave number can be recognized. This is the band dispersion for heterostructure A with a deposition time of 3 min. After further deposition (8 min), the band dispersion changes significantly as the originally buried and unclear Dirac point now becomes apparent, as shown in Fig. 1(c) (heterostructure B). We previously performed an extensive study on heterostructure B and revealed that it is a mixed phase composed of MnBi₂Te₄/Bi₂Te₃ and Mn₄Bi₂Te₇/Bi₂Te₃ [19]. In short, these compounds are heterostructures with one and four MnTe layers inserted inside the topmost Bi₂Te₃ quintuple layer, respectively. The mixed-phase nature of heterostructure B was also revealed in the LEED patterns taken at 100 K, as shown in Figs. 1(d)-1(f). Whereas that of heterostructure A shown in Fig. 1(d) reveals only sharp single spots, a satellite feature with a slightly different lattice constant can additionally be found for heterostructure B [Fig. 1(e)], as clearly revealed in Fig. 1(f) [30]. Since heterostructure A seems to be a single phase containing less Mn than heterostructure B, it is most likely the MnBi₂Te₄/Bi₂Te₃ heterostructure.

To prove the above expectation, LEED *I-V* measurements were performed. LEED patterns with incident energy from 30 to 400 eV were recorded in steps of 1 eV by a digital CCD camera at 100 K, as shown by the red curves in Fig. 2(a) [31]. In order to determine the surface structure, we calculated the I-V curves in the tensor LEED to fit the experimental I-V curves using the SATLEED package of Barbieri and Van Hove and minimized Pendry's R factor R_n [32]. As shown in Fig. 2(b), each atomic layer was treated differently according to their environments. Angular momentum up to 17 (l_{max} = 17) was taken into account because of the strong scattering of the heavy Bi atom (Z = 83). Considering the mean penetration depth of the incident electrons of ~ 10 Å, only the topmost seven surface layers were allowed to relax, and we used the bulk Bi₂Te₃ parameters for the layers beneath. In the search for the optimal structure, the Debye temperature of each atom was changed in steps of 10 K from 50 up to 300 K. The optimized structure with the determined parameters is shown in Fig. 2(b). The experimental and theoretical I-V curves agree well with $R_p = 0.28 \pm 0.04$. As a result, we can say that heterostructure A is, indeed, the MnBi₂Te₄/Bi₂Te₃ heterostructure in accordance with our expectation. One can also say that there is negligible surface relaxation in the

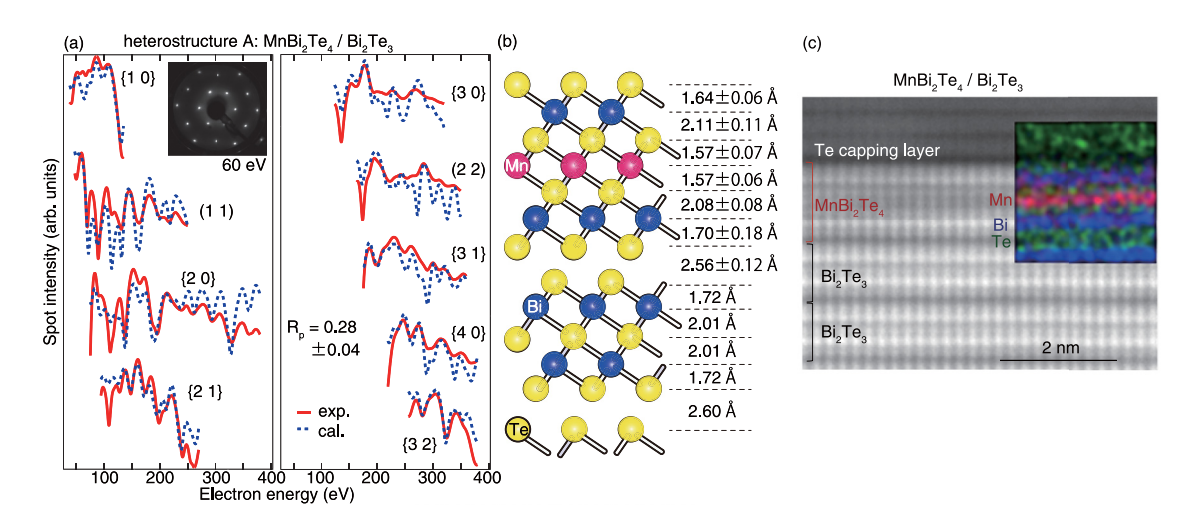


FIG. 2. (a) Experimental I-V spectra of LEED spots at 100 K for heterostructure A and the calculated spectra of the optimized model shown in (b). The inset shows the LEED pattern at 60 eV. (b) Cross-sectional view of the optimized model of heterostructure A with the determined interlayer spacings indicated. The structure is $MnBi_2Te_4/Bi_2Te_3$. (c) HAADF-STEM image of the heterostructure measured at room temperature. The electron beam was incident along the [110] direction.

surface layers from the determined lattice parameters, similar to the case for pure Bi₂Te₃ [33].

To gain further evidence, we performed STEM measurements. Figure 2(c) shows the high-angle annular dark field STEM (HAADF-STEM) observation from the [110] direction. EDS measurements were also performed to verify the atomic composition, as shown in the inset. From these data, there is no doubt that the heterostructure is MnBi₂Te₄/Bi₂Te₃, although intermixing between Mn and Bi can slightly be seen.

After the atomic structure of MnBi₂Te₄/Bi₂Te₃ (we will refer to it as MBT/BT from now on) was unambiguously determined, XMCD measurements were performed to verify the magnetic properties of this MBT/BT heterostructure. Figure 3(a) shows the XAS spectra taken at 5.6 K with a magnetic field of 10 T applied perpendicular to the sample at the Mn L edge. μ_+ and μ_- correspond to the spectrum obtained with left- and right-handed circularly polarized photons, respectively. The corresponding XMCD spectrum is also shown, and a clear signal is detected. Figure 3(b) shows the magnetic field dependence of the XMCD spectra. The peak signal decreases for smaller fields. The inset shows the enlarged spectra at zero field, showing no significant signal compared to the background. This means that there is no remanent magnetization in this system.

To gain further insight into the magnetism of this system, detailed field-dependent measurements were conducted, as shown in Fig. 3(c) (M-H curves). The L_3 peak intensity at 639.8 eV was measured, and the background signal was subtracted, which is the average intensity at 635, 637, 645, and 648 eV. The magnetic field was swept as $+3 \rightarrow 0 \rightarrow -3 \rightarrow 0 \rightarrow +3$ T. One can obviously see that the XMCD signal shows a linear dependence on the applied magnetic field. This again shows that the system is paramagnetic at 5.6 K, the lowest temperature we were able to reach. In order to obtain further evidence of the paramagnetic nature of the system, we have measured the temperature dependence of the XMCD signal up to 210 K at a field of 2 T, as shown in Fig. 3(d). The

data can be fitted by Curie's law, $M \propto \frac{A}{T}$, as shown by the red solid line. This unambiguously confirms that the MBT/BT system is paramagnetic and does not show ferromagnetism down to 5.6 K.

Finally, high-resolution ARPES measurements were performed to clarify the relationship between the absence and formation of the DC gap and the magnetic property in the MBT/BT system. Figure 4(b) shows the band dispersion

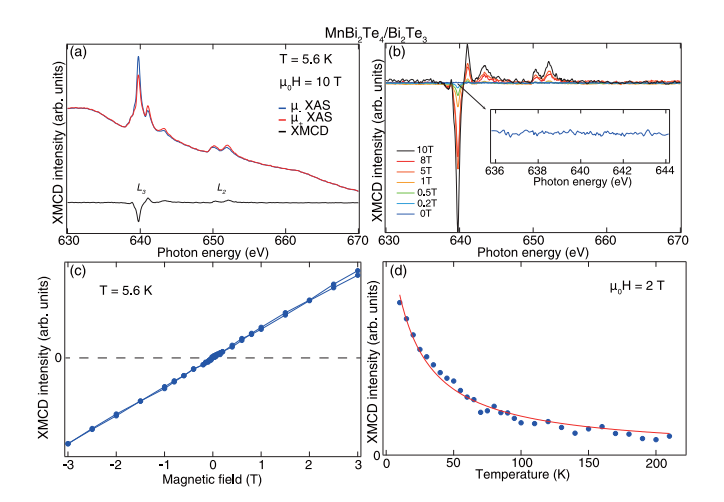


FIG. 3. (a) X-ray absorption spectra (XAS) of MnBi $_2$ Te $_4$ /Bi $_2$ Te $_3$ measured at 5.6 K for a circularly polarized incident light when a ± 10 T magnetic field was applied along the sample surface-normal direction. μ_+ and μ_- correspond to the spectrum obtained with left- and right-handed circularly polarized photons, respectively. The corresponding XMCD spectrum is also shown. The Te capping layer was removed by annealing the sample in UHV. (b) Magnetic field dependence of the XMCD spectra. The inset shows the enlarged spectra at zero field, showing no significant signal compared to the background. (c) Magnetic field dependence of the XMCD signal (639.8 eV) measured at 5.6 K. (d) Temperature dependence of the XMCD signal measured with a magnetic field of 2 T.

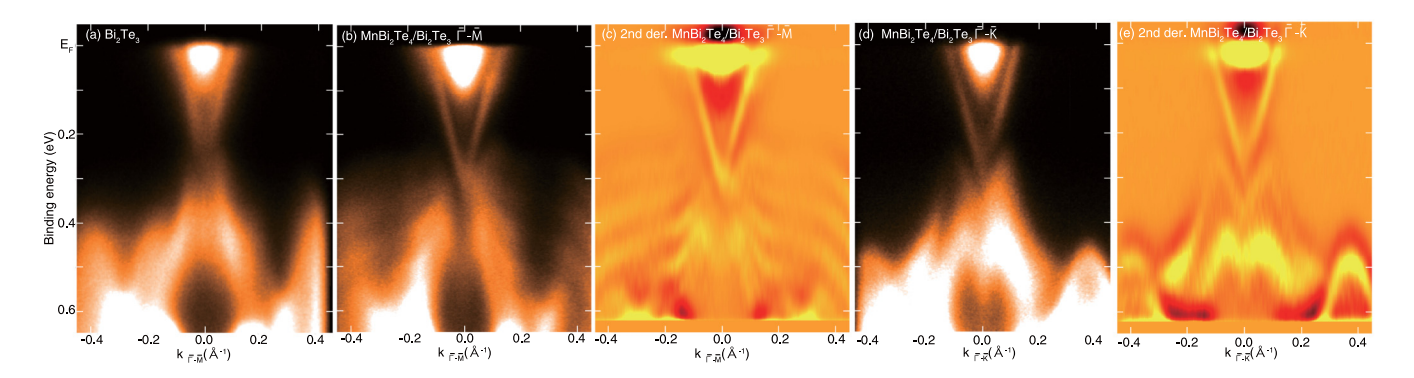


FIG. 4. (a) The band structure of the substrate Bi_2Te_3 film and (b) that of the heterostructure $MnBi_2Te_4/Bi_2Te_3$ along the $\bar{\Gamma}$ - \bar{M} direction; the measurements were performed at 16 K with $h\nu=19$ eV. (c) The second derivative with respect to the energy of the band dispersion image shown in (b). (d) and (e) Same as (b) and (c), but along the $\bar{\Gamma}$ - \bar{K} direction. The measurements were performed at 16 K with $h\nu=18$ eV.

measured with hv = 19 eV photons at 16 K along the $\bar{\Gamma}$ - \bar{M} direction. Compared to the pristine Bi₂Te₃ shown in Fig. 4(a), one can notice that the Dirac point has shifted down to higher binding energy and the Fermi wavelength has increased slightly. When one focuses on the regions at wave numbers larger than 0.2 Å^{-1} below 0.3 eV, one can find "skeletonlike" features that can clearly be seen in the second derivative image in Fig. 4(c). These features are absent in Fig. 4(a) and can be attributed to the heterostructure formation. Thus, there seems to be some change in the band dispersion by the incorporation of Mn and Te, although it is not very prominent. Figure 4(d) shows the band dispersion of MBT/BT along the $\bar{\Gamma}$ - \bar{K} direction measured with $h\nu = 18$ eV photons at 16 K. The skeletonlike feature is absent, and one can notice that a single band is dispersing downwards in this direction, which can clearly be noticed by the second derivative image in Fig. 4(e).

The most significant characteristic of the DC dispersion of MBT/BT in Figs. 4(b) and 4(d) is that there is little change from the original Bi₂Te₃, which suggests that there is no clear gap feature. In Ref. [19], a mixed sample composed of both MBT/BT and Mn₄Bi₂Te₇/Bi₂Te₃ was studied extensively. The band dispersion shown in Figs. 4(b)-4(e) is consistent with the additional feature observed outside the gapped DC in Ref. [19] in some measurement conditions. (The gapped DC was attributed to the latter heterostructure [19].) Thus, the results shown in Figs. 4(b)-4(e) can be said to represent the whole band dispersion of MBT/BT that was missing in Ref. [19] and show that the DC of MBT/BT is massless down to 16 K. We should also mention that the Mn in MBT/BT was also concluded to be paramagnetic down to 6 K in this mixed sample from XMCD measurements [19]. Thus, we believe that the fact that MBT/BT is paramagnetic is supported by multiple sources of experimental evidence measured with ARPES and XMCD. This result is in clear contrast to the calculated band dispersion of MBT/BT shown in Ref. [13], where a DC gap of 77 meV opened due to the time-reversal symmetry breaking of the ferromagnetic Mn layer. However, when we compare the experimentally determined band dispersion with the results of ab initio calculation for MBT/BT in the wider range of E-k space shown in Fig. 3(a) of Ref. [19], it can be said that the experiment and the calculation are consistent with each other except for the presence or absence of the DC gap since the skeletonlike bands also appear along the $\bar{\Gamma}$ - \bar{M} direction in the calculation. It should also be noted that these skeletonlike bands are mostly localized at the topmost MBT and have their maximum contribution from the Mn p_z orbital in this calculation, and we speculate that this is the reason why they appeared clearly in the experiment only after the formation of the MBT/BT heterostructure. Furthermore, there is only a single band that disperses downwards along the $\bar{\Gamma}$ - \bar{K} direction in this calculation, which is also consistent with the observation in Figs. 4(d) and 4(e).

Let us now discuss the present result by comparing it with other materials based on MBT. For bulk MnBi₂Te₄, the Néel temperature is reported to be 25 K [15]. The critical temperature for $(MnBi_2Te_4)(Bi_2Te_3)_m$ (m = 2-6) has been reported to be more or less around 10 K [34]. In Ref. [35], it was predicted that the Curie temperature of freestanding MnBi₂Te₄ is 12 K from Monte Carlo simulations and nearly 20 K from density functional theory calculations combined with self-consistent spin-wave theory [36]. These values are higher than the lowest temperature we have achieved in our XMCD measurements. In a recent study, ferromagnetism was actually observed in exfoliated MnBi₂Te₄ flakes down to the single septuple layer, and the Curie temperature was reported as 15 K [27]. This is somewhat different from the present results, in which the Curie temperature should be lower than 6 K. One of the possible origins of this discrepancy is the difference in the substrate (Au in Ref. [27] but BT in the present study), pointing to the importance of the role of the substrate in the magnetic properties. A second reason may be the difference in the probing spot size for magnetic characterization (2 μ m in Ref. [27] but 200 μ m in the present XMCD measurements) since 2D magnets can show the domain structure at remanence [37]. Another may be the slight intermixing between Bi and Mn in the present samples. All in all, the present situation is similar to the case of VSe₂, for which the absence or presence of ferromagnetism has been intensively debated.

We would like to note that the presence of multiple Mn stacks within the sample may still be a key factor to stabilize the magnetic state, although the interaction between adjacent Mn layers may be quite weak. In this respect, one needs to keep in mind that it has been reported that the Dzyaloshinskii-Moriya interaction mediated by the surface states can play a crucial role in magnetic topological heterostructures to

induce an emergent magnetic field. This results in the observation of the topological Hall effect due to the formation of skyrmions [38,39]. This kind of interlayer interaction among multiple magnetic layers may also be important in stabilizing the ferromagnetic state, and it would be interesting to make multiple layers of MBT on BT and investigate its magnetic properties as well as the relation to the surface DC dispersion.

Finally, we compare the present results with the case of the MnBi₂Se₄/Bi₂Se₃ (MBS/BS) heterostructure. In MBS/BS, a clear DC gap of ~100 meV was observed, and its ferromagnetic nature was confirmed with magnetic measurements [12]. The experimentally determined band structure was also consistent with that from ab initio calculations assuming an out-of-plane magnetic moment in the Mn layer. These facts are in contrast to the present situation for MBT/BT, where the Dirac-cone gap as well as the ferromagnetic order is missing down to 5.6 K. While it is difficult to make a clear explanation concerning the drastic difference in the two heterostructures, the weaker spin-orbit coupling of Se compared to Te may be one factor. It has been shown that in MBT/BT, the singleion anisotropy dominates, while in MBS/BS, the exchange anisotropy and the single-ion anisotropy both play key roles in the magnetic interaction [36]. A delicate balance between the two may result in a robust long-range magnetic order in MBS/BS. Further study is needed to clarify the intriguing properties of these 2D vdW materials.

- [1] C. Gong, L. Li, Z. Li, H. Ji, A. Stern, Y. Xia, T. Cao, W. Bao, C. Wang, Y. Wang, Z. Q. Qiu, R. J. Cava, S. G. Louie, J. Xia, and X. Zhang, Nature (London) 546, 265 (2017).
- [2] B. Huang, G. Clark, E. Navarro-Moratalla, D. R. Klein, R. Cheng, K. L. Seyler, D. Zhong, E. Schmidgall, M. A. McGuire, D. H. Cobden, W. Yao, D. Xiao, P. Jarillo-Herrero, and X. Xu, Nature (London) 546, 270 (2017).
- [3] K. Burch, D. Mandrus, and J. Park, Nature (London) 563, 47 (2018).
- [4] M. Gibertini, M. Koperski, A. F. Morpurgo, and K. S. Novoselov, Nat. Nanotechnol. 14, 408 (2019).
- [5] K. Xu, P. Chen, X. Li, C. Wu, Y. Guo, J. Zhao, X. Wu, and Y. Xie, Angew. Chem., Int. Ed. 52, 10477 (2013).
- [6] M. Bonilla, S. Kolekar, Y. Ma, H. Diaz, V. Kalappattil, R. Das, T. Eggers, H. Gutierrez, M. Phan, and M. Batzill, Nat. Nanotechnol. 13, 289 (2018).
- [7] J. Feng et al., Nano Lett. 18, 4493 (2018).
- [8] P. Chen, W. W. Pai, Y.-H. Chan, V. Madhavan, M. Y. Chou, S.-K. Mo, A.-V. Fedorov, and T.-C. Chiang, Phys. Rev. Lett. 121, 196402 (2018).
- [9] M. Nakano, Y. Wang, S. Yoshida, H. Matsuoka, Y. Majima, K. Ikeda, Y. Hirata, Y. Takeda, H. Wadati, Y. Kohama, Y. Ohigashi, M. Sakano, K. Ishizaka, and Y. Iwasa, Nano Lett. 19, 8806 (2019).
- [10] M. Mogi, T. Nakajima, V. Ukleev, A. Tsukazaki, R. Yoshimi, M. Kawamura, K. S. Takahashi, T. Hanashima, K. Kakurai, T. H. Arima, M. Kawasaki, and Y. Tokura, Phys. Rev. Lett. 123, 016804 (2019).
- [11] S. V. Eremeev, M. M. Otrokov, and E. V. Chulkov, J. Alloys Compd. 709, 172 (2017).

IV. CONCLUSION

In summary, we succeeded in fabricating the $MnBi_2Te_4/Bi_2Te_3$ heterostructure and measured its electronic structure with ARPES and is magnetic properties with XMCD. In contrast to the previous calculation and experimental works on related materials, the system was paramagnetic down to 5.6 K. Our results call for further studies on the intricate magnetic properties of 2D van der Waals topological heterostructures.

ACKNOWLEDGMENTS

The authors thank M. M. Otrokov, S. V. Eremeev, E. V. Chulkov, T. Takashiro, and R. Akiyama for stimulating discussions. T. T. Sasaki and K. Hono are acknowledged for their help with the STEM measurements. T. Shirasawa and Y. Ohtsubo are acknowledged for their help with the setup of the LEED *I-V* measurement system. This work was supported by Grants-In-Aid from the JSPS KAKENHI (Grant No. 18H03877), the Murata Science Foundation (Grant No. H30-084), the Asahi Glass Foundation, the Iketani Science and Technology Foundation (Grant No. 0321083-A), and a Tokyo Tech Challenging Research Award. The ARPES measurements were performed under UVSOR Proposals No. 29-837, No. 30-571, No. 30-860, No. 19-569, and No. 19-858. The XMCD measurements were performed under SPring-8 Proposals No. 2018B3843 and No. 2019B3843.

- [12] T. Hirahara, S. V. Eremeev, T. Shirasawa, Y. Okuyama, T. Kubo, R. Nakanishi, R. Akiyama, A. Takayama, T. Hajiri, S.-I. Ideta, M. Matsunami, K. Sumida, K. Miyamoto, Y. Takagi, K. Tanaka, T. Okuda, T. Yokoyama, S.-I. Kimura, S. Hasegawa, and E. V. Chulkov, Nano Lett. 17, 3493 (2017).
- [13] M. M. Otrokov, T. V. Menshchikova, M. G. Vergniory, I. P. Rusinov, A. Y. Vyazovskaya, Y. M. Koroteev, G. Bihlmayer, A. Ernst, P. M. Echenique, A. Arnau, and E. V. Chulkov, 2D Mater. 4, 025082 (2017).
- [14] M. M. Otrokov, T. V. Menshchikova, I. P. Rusinov, M. G. Vergniory, V. M. Kuznetsov, and E. V. Chulkov, JETP Lett. 105, 297 (2017).
- [15] M. M. Otrokov et al., Nature (London) 576, 416 (2019).
- [16] Y. Gong et al. Chin. Phys. Lett. 36, 076801 (2019).
- [17] S. V. Eremeev, M. M. Otrokov, and E. V. Chulkov, Nano Lett. 18, 6521 (2018).
- [18] Y. Li, Y. Jiang, J. Zhang, Z. Liu, Z. Yang, and J. Wang, Phys. Rev. B **102**, 121107(R) (2020).
- [19] T. Hirahara, M. M. Otrokov, T. T. Sasaki, K. Sumida, Y. Tomohiro, S. Kusaka, Y. Okuyama, S. Ichinokura, M. Kobayashi, Y. Takeda, K. Amemiya, T. Shirasawa, S. Ideta, K. Miyamoto, K. Tanaka, S. Kuroda, T. Okuda, K. Hono, S. V. Eremeev, and E. V. Chulkov, Nat. Commun. 11, 4821 (2020).
- [20] J. Wu, M. Sasase, K. Ienaga, Y. Obata, R. Yukawa, K. Horiba, H. Kumigashira, S. Okuma, T. Inoshita, and H. Hosono, Sci. Adv. 5, eaax9989 (2019).
- [21] Y.-J. Hao et al., Phys. Rev. X 9, 041038 (2019).
- [22] H. Li et al., Phys. Rev. X 9, 041039 (2019).
- [23] Y. J. Chen, L. X. Xu, J. H. Li, Y. W. Li, H. Y. Wang, C. F. Zhang, H. Li, Y. Wu, A. J. Liang, C. Chen, S. W. Jung, C. Cacho, Y. H.

- Mao, S. Liu, M. X. Wang, Y. F. Guo, Y. Xu, Z. K. Liu, L. X. Yang, and Y. L. Chen, Phys. Rev. X 9, 041040 (2019).
- [24] B. Chen et al. Nat. Commun. 10, 4469 (2019).
- [25] P. Swatek, Y. Wu, L.-L. Wang, K. Lee, B. Schrunk, J. Yan, and A. Kaminski, Phys. Rev. B 101, 161109(R) (2020).
- [26] S. H. Lee, Y. Zhu, Y. Wang, L. Miao, T. Pillsbury, H. Yi, S. Kempinger, J. Hu, C. A. Heikes, P. Quarterman, W. Ratcliff, J. A. Borchers, H. Zhang, X. Ke, D. Graf, N. Alem, C.-Z. Chang, N. Samarth, and Z. Mao, Phys. Rev. Res. 1, 012011(R) (2019).
- [27] S. Yang, X. Xu, Y. Zhu, R. Niu, C. Xu, Y. Peng, X. Cheng, X. Jia, Y. Huang, X. Xu, J. Lu, and Y. Ye, Phys. Rev. X 11, 011003 (2021).
- [28] S.-I. Kimura, T. Ito, M. Sakai, E. Nakamura, N. Kondo, T. Horigome, K. Hayashi, M. Hosaka, M. Katoh, T. Goto, T. Ejima, and K. Soda, Rev. Sci. Instrum. 81, 053104 (2010).
- [29] Y. Takeda, M. Kobayashi, T. Okane, T. Ohkochi, J. Okamoto, Y. Saitoh, K. Kobayashi, H. Yamagami, A. Fujimori, A. Tanaka, J. Okabayashi, M. Oshima, S. Ohya, P. N. Hai, and M. Tanaka, Phys. Rev. Lett. 100, 247202 (2008).
- [30] See Supplemental Material at http://link.aps.org/supplemental/ 10.1103/PhysRevB.103.205405 for information on the LEED *I-V* curve of the (20) spot for samples with controlled deposition time to support the fact that heterostructure A is a single phase, whereas the samples with larger deposition time are a mixed phase.
- [31] The symmetrically inequivalent spots, such as (10) and (01), exhibited almost the same I-V curves. Since this feature was

- also seen for the pristine $\mathrm{Bi}_2\mathrm{Te}_3$ LEED patterns, it comes from the fact that there are twin domains on the surface that are related by a 180° rotation. The superposition of the two domains should lead to the apparent twofold symmetry. Taking this double-domain surface into account, we took the average of the *I-V* curves both in the calculation and in the experimental data such that $\{hk\}$ is the average of (hk) and (kh) spots [see Fig. 2(a)]. Note that spots having the same mirror indices of h and k do not need averaging.
- [32] M. A. Van Hovea, W. Moritz, H. Over, P. J. Rous, A. Wander, A. Barbieri, N. Materer, U. Starke, and G. A. Somorjai, Surf. Sci. Rep. 19, 191 (1993).
- [33] N. Fukui, T. Hirahara, T. Shirasawa, T. Takahashi, K. Kobayashi, and S. Hasegawa, Phys. Rev. B 85, 115426 (2012).
- [34] I. I. Klimovskikh et al., npj Quantum Mater. 5, 54 (2020).
- [35] M. M. Otrokov, I. P. Rusinov, M. Blanco-Rey, M. Hoffmann, A. Yu. Vyazovskaya, S. V. Eremeev, A. Ernst, P. M. Echenique, A. Arnau, and E. V. Chulkov, Phys. Rev. Lett. 122, 107202 (2019).
- [36] Y. Li, Z. Jiang, J. Li, S. Xu, and W. Duan, Phys. Rev. B 100, 134438 (2019).
- [37] T. Taniuchi, Y. Motoyui, K. Morozumi, T. C. Rödel, F. Fortuna, A. F. Santander-Syro, and S. Shin, Nat. Commun. 7, 11781 (2016).
- [38] K. Yasuda, R. Wakatsuki, T. Morimoto, R. Yoshimi, A. Tsukazaki, K. S. Takahashi, M. Ezawa, M. Kawasaki, N. Nagaosa, and Y. Tokura, Nat. Phys. 12, 555 (2016).
- [39] T. Takashiro, R. Akiyama, I. A. Kibirev, A. V. Mateskiy, R. Nakanishi, S. Sato, T. Fukasawa, T. Sasaki, K. Hono, H. Toyama, K. Hiwatari, A. V. Zotov, A. A. Saranin, T. Hirahara, and S. Hasegawa (unpublished).